Macromolecules
ARTICLE

Macromolecules **2009**, *42*, 6999–7007 **6999**
DOI: 10.1021/ma901227k

Photochemically Cross-Linked Perfluoropolyether-Based Elastomers: Synthesis, Physical Characterization, and Biofouling Evaluation

Zhaokang Hu,[†] John A. Finlay,[§] Liang Chen,[⊥] Douglas E. Betts,[†] Marc A. Hillmyer,[⊥] Maureen E. Callow,[§] James A. Callow,[§] and Joseph M. DeSimone*[,†,‡]

[†]*Department of Chemistry, University of North Carolina at Chapel Hill, Chapel Hill, North Carolina 27599,* [‡]*Department of Chemical Engineering, North Carolina State University, Raleigh, North Carolina 27695,* [§]*School of Biosciences, University of Birmingham, Birmingham B15 2TT, U.K., and* [⊥]*Department of Chemistry, University of Minnesota, Minneapolis, Minnesota 55455*

Received February 12, 2009; Revised Manuscript Received August 9, 2009

ABSTRACT: A series of reactive liquid perfluoropolyether (PFPE) precursors were synthesized which can be photochemically cross-linked (UV-cured) into high-performance PFPE elastomers in one step. To investigate how fundamental changes in the PFPE molecular structure correlate to bulk and surface properties, the variable functional end group, molecular weight, and the copolymer content were systematically explored in relation to thermal stability, contact angle/surface tension, modulus, and biofouling behavior. The morphologies of these PFPE materials were studied using differential scanning calorimetry, dynamic mechanical thermal analysis, and small-angle X-ray scattering. From these studies, it was determined that clusters of polymerized functional end groups were found to be nanophase separated within the PFPE matrix. By varying the cross-link density, the Young's modulus of the fully cross-linked PFPE elastomeric film could be tuned from 1.5 to 90 MPa with a critical surface tension of 8.6−16 mN/m. The marine antifouling and fouling-release properties of the cross-linked PFPE elastomeric coatings were evaluated by settlement and release assays involving zoospores and sporelings (young plants), respectively, of green fouling alga *Ulva*.

Introduction

Tailored polymeric materials have been studied as leading candidates for marine antifouling/fouling-release coatings since the ban of traditional antifouling coatings containing tributyltin compounds (TBT).[1] Most of the efforts to design environmentally benign coatings have focused on improving polydimethylsiloxane (PDMS).[2−6] Baier and Brady et al. indicated that the relative adhesion on different polymeric surfaces decreased linearly with decreasing surface energy down to ∼25 mN/m.[7,8] Combining low modulus (2.4 MPa for fully cured Sylgard 184) with low surface tension (∼25 mN/m), flexible PDMS elastomers have proven to be promising fouling-release materials.[8,9] Accumulated fouling organisms are readily "released" from these coatings by hydrodynamic forces, such as those generated by a ship moving through water. However, it is well-known that PDMS is not compatible with many organic solvents and lipid-rich materials. As a result, PDMS coatings are prone to swelling that leads to premature mechanical failure, severely limiting the use of these materials in many applications.[10] Furthermore, PDMS-based fouling release coatings accumulate slime dominated by algal cells, which are not "released" by the hydrodynamic conditions generated by the majority of vessels. Such slimes impose significant hydrodynamic drag on vessels moving through the water.[11]

In an effort to address this concern, a number of researchers have made progress toward next-generation fouling-release coatings by investigating fluorinated polymeric materials. The incorporation of fluorinated groups into a polymeric matrix is very attractive because of their unique properties, such as chemical and thermal stability in various environments, as well as good weathering resistance, low surface tension, hydrophobicity, and oleophobicity.[12] Recent work by Wooley et al. has shown that a hyperbranched fluoropolymer matrix with cross-linked poly(ethylene glycol) (PEG) performed well as a fouling-release coating.[13] A class of comblike amphiphilic graft copolymers discovered by Ober et al. that are composed of PEGylated perfluoroalkyl side chains demonstrated low adhesion strength to both the green macroalga, *Ulva*, and the slime-forming diatom, *Navicula*.[14,15] Furthermore, a fluorinated silicone has been synthesized by Chaudhury et al. as a fouling-release coating with tunable release properties by reacting an allylamide-terminated perfluoropolyether oligomer with silicone via a platinum-catalyzed hydrosilylation reaction. This material has not been evaluated yet for its resistance to biofouling,[16] but fluorinated-silicone copolymer blends have recently been shown in laboratory assays to have improved fouling-release properties for both algae and barnacles compared to silicone alone.[17] Early work by our group demonstrated the synthesis of a series of thermally cross-linkable perfluoropolyether (PFPE) graft terpolymers containing various alkyl (meth)acrylate monomers with glycidyl methacrylate as a cure-site monomer, showing promise as both antifouling and fouling-release materials.[18] While these fluorinated polymers showed improved biofouling performance as marine coatings compared to a standard PDMS elastomeric coating, most of them involved either multistep reactions or complicated surface modifications. More recently, our group optimized the synthesis of functionalized PFPEs via a photochemical cross-linking (UV curing) process with the practical ease of solventless processability. The advantages offered by the UV curing technique are of great interest in coating operations

*To whom correspondence should be addressed: e-mail desimone@unc.edu.

Published on Web 08/28/2009

Scheme 1. Chemical Structures of PFPE Macromonomers: (a) 1 or 4 kg/mol PFPE-DMA, (b) 2 × 4 kg/mol PFPE-DMA, (c) 3 × 4 kg/mol PFPE-DMA, (d) 4 kg/mol sPFPE, and (e) Fluorinated Styrenesulfonic Ester (SS)

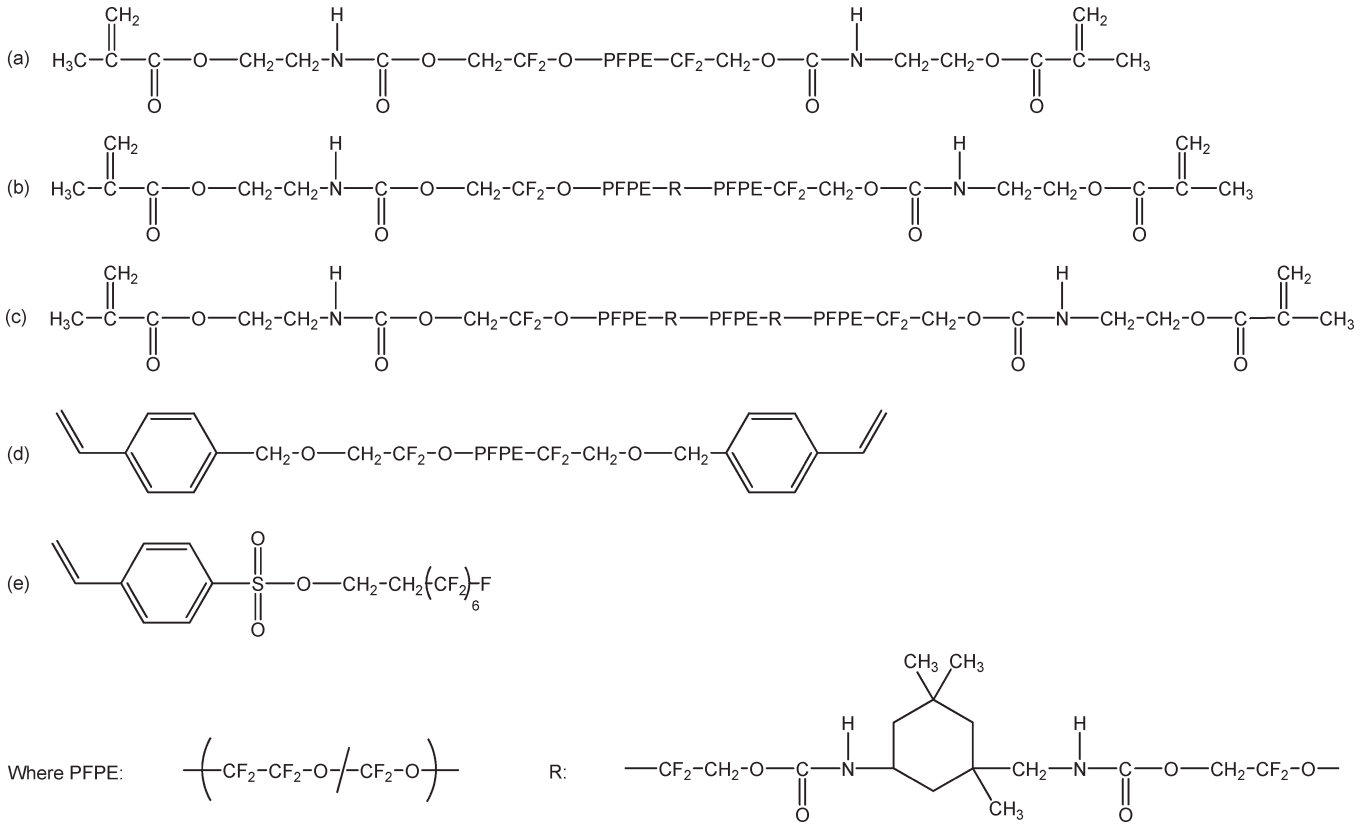

because they do not require the use of solvents, can be complete in a few seconds, are energy efficient, and use simple equipment.[19,20] This article reports the synthesis and characterization of a series of photochemically cured PFPE-based elastomeric networks. In order to investigate the structure/property relationships, different functional end groups such as methacrylate and styrene were used to modify the PFPE diol precursors of variable molecular weight to form cross-linkable difunctional PFPE macromonomers. A distyrenyl PFPE/styrenesulfonic ester copolymer network (sPFPE-SS) was also prepared by photochemically cross-linking a blend of distyrenyl-modified PFPE (sPFPE) with a fluorinated derivative of a styrenesulfonic ester monomer (SS) to study its effect on the mechanical and surface properties. The properties of these materials including the thermal stability, modulus, contact angle, surface tension, and antifouling/fouling-release performance were systematically studied.

Experimental Section

Materials. The solvent 1,1,1,3,3-pentafluorobutane (Solkane 365 MFC) was purchased from Micro-Care and used as received. The 1 and 4 kg/mol PFPE diols (Fluorolink D10 and Fomblin ZDOL 4000, respectively) were purchased from Solvay Solexis. The 4-vinylbenzenesulfonyl chloride monomer was purchased from TCI America. All the other chemicals were purchased from Aldrich and used as received.

Synthesis of α,ω-Dimethacrylate-Modified Perfluoropolyether Macromonomers (PFPE-DMA). The synthesis of the PFPE-DMA macromonomer has been reported previously.[21] Briefly, telechelic PFPE diol was first dissolved in 1,1,1,3,3-pentafluorobutane and allowed to react with an 1:2.05 molar ratio of 2-isocyanatoethyl methacrylate (IEM) at 45 °C for 24 h, using 0.1 wt % tetrabutyltin diacetate (DBTDA) as a catalyst. The solution was then passed through a chromatographic column filled with alumina (2 × 10 cm). The photoinitiator, α-hydroxycyclohexyl phenyl ketone (HCPK, 0.2 wt %), was added, and the solvent was subsequently removed by rotoevaporation. The product was filtered through a 0.2 μm filter to yield a clear, colorless, viscous oil (Scheme 1). To obtain the chain extended 2 × 4 and 3 × 4 kg/mol PFPE-DMA macromonomers, the 4 kg/mol PFPE diol was first reacted with isophorone diisocyanate (IPDI) in a proper stoichiometry to yield the chain extended PFPE diols.[22] The compound with diol end groups were then modified with IEM to form the dimethacrylate-modified macromonomers as described above.

Synthesis of α,ω-Distyrenyl-Modified Perfluoropolyether Macromonomer (sPFPE). The sPFPE was synthesized by the following procedure.[23] In a typical synthesis, 30 g of the 4 kg/mol PFPE diol (7.89 mmol) and 1.5 g of tetrabutylammonium hydrogen sulfate (4.42 mmol) were first dissolved in 60 mL of 1,1,1,3,3-pentafluorobutane. Potassium hydroxide (15 g, 0.27 mol) dissolved in 30 mL of deionized water was then added under stirring, which was followed by the addition of 3 mL of 4-vinylbenzyl chloride (19.2 mmol). The yellow mixture was reacted under vigorous stirring at 45 °C for 48 h. After filtering out the brown solids, the product was washed with deionized water three times and then decolorized by stirring over activated carbon overnight. After filtering out the activated carbon with a 0.2 μm filter, evaporation of the solvent yielded a clear, colorless, viscous oil.

Synthesis of Fluorinated Styrenesulfonic Ester Monomer (SS). In order to make styrenesulfonic ester compatible with sPFPE, a fluorinated tail was added to 4-vinylbenzenesulfonyl chloride.[23] To a 150 mL round-bottom flask, 3,3,4,4,5,5,6,6,7,7,8,8,8-tridecafluoro-1-octanol (13.66 g, 37.5 mmol), triethylamine (10 mL), pyridine (20 mL), and 4-vinylbenzenesulfonyl chloride (7.6 g, 37.5 mmol) were added. The resulting slurry was stirred at room temperature for 20 h under argon flow. The reaction mixture was then poured into a dilute hydrochloric acid ice bath to quench the remaining triethylamine and pyridine. The aqueous solution was extracted with diethyl ether three times, and the

combined ether layer was washed sequentially with water, 10% NaOH solution, and 10% NaCl solution. The ether solution was then dried over $MgSO_4$ for 1 h. After removing the $MgSO_4$ and solvent, the dry product was recovered as a waxy light yellow solid.

Photocure of PFPE Precursors. In a typical cure, 0.2 wt % of HCPK was first added to the PFPE macromonomers. The elastomeric films were formed by casting the PFPE macromonomers over a silicon wafer followed by UV irradiation (Electronlite UV curing chamber model no. 81432-ELC-500, $\lambda = 365$ nm) under nitrogen purge for 10 min ($\sim$38 000 mJ/cm^2). To fabricate the sPFPE-SS copolymer network, the 4 kg/mol sPFPE macromonomer with 0.2 wt % of HCPK and the fluorinated styrenesulfonic ester comonomer were mixed in the desired weight ratio (10% fluorinated styrenesulfonic ester in this study). The mixture was first heated above 40 °C to form a homogeneous solution and then photochemically cured as described previously.

Thermal Analysis. The thermal stability of the cured PFPE elastomers was investigated with a Perkin-Elmer Pyris I thermogravimetric analyzer (TGA). Fully cured films were first predehydrated in a vacuum oven at 110 °C overnight to remove any residual moisture and then heated from 25 to 600 °C in a nitrogen atmosphere with a heating rate of 10 °C/min. The temperature at 5% weight loss was defined as the decomposition temperature. Differential scanning calorimetry (DSC) curves were recorded on a Seiko DSC 220 in the temperature of −150 to 100 °C at a scanning rate of 10 °C/min. Dynamic mechanical thermal analysis (DMTA) was performed using a PerkinElmer Pyris Diamond DMA 6100 at a fixed frequency of 1 Hz in tension mode. The program temperature was varied from −150 to 150 °C with a heating rate of 2 °C/min.

Small-Angle X-ray Scattering (SAXS). The SAXSess instrument (Anton Paar) at the University of Minnesota was utilized to probe the microstructure in the fully cured PFPE elastomeric films. The film was placed in a copper sample holder, and the scattering was measured at room temperature for 5 min operating at 40 kV and 50 mA. The scattering signals were not corrected for instrumental broadening caused by the line-collimated incident beam but were integrated into a 1D plot of intensity versus the scattering vector, q. Finally, the scattering intensity was normalized with respect to the incident beam intensity.

Mechanical Properties. Stress−strain measurements were performed using rectangular samples ($1 \times 10 \times 20$ mm) at ambient temperature on an Instron model 5566 system using a 10 kN load cell at a crosshead speed of 5 mm/min. An extensiometer of 15 mm gauge length was used to measure the strain accurately. From the stress−strain curves, the Young's modulus was calculated. Four replicates were performed for each sample.

Control of Relative Humidity at the Time of Cure. To control the humidity in the UV cure oven, a humidified nitrogen stream was used to purge the chamber environment while curing. The nitrogen stream was humidified by first passing the gas through a bubbler containing LiCl aqueous solutions at varying concentrations.[24] Humidities of 19%, 42%, 58%, and 76% were generated by this method. A 100% humidity environment was induced by passing the nitrogen stream through a bubbler containing deionized water. The 0% relative humidity environment was obtained by passing the nitrogen stream through a Drierite desiccant tube that was prebaked in a heating oven at 110 °C for 24 h, and all connecting tubes were predried in a vacuum oven for 24 h. A digital humidity meter was placed at the nitrogen outlet of the UV oven to monitor the real time humidity during the entire curing process. Once the desired humidity inside the UV chamber was reached, typically after 15−20 min of purging, the samples were cured by UV irradiation for 10 min under the continuous nitrogen stream.

Surface Analysis. Dynamic tensiometry measurements were performed on a NIMA Technologies DST 9005 dynamic surface tensiometer. PFPE thin films on glass coverslips measuring $22 \times 22 \times 0.1$ mm were formed by dip-coating the coverslips in the pure the PFPE liquid macromonomers followed by UV curing as previously described. The dynamic contact angle was measured by the Wilhelmy plate method.[25] Typically, a PFPE dip-coated glass coverslip was attached to an electrobalance via a clip, and a stage with a dish of pure solvent (water) was automatically raised and lowered to allow the solvent to impinge upon the slide at a speed of 5 mm/min. The advancing and receding contact angles were recorded when the samples were immersed into and departing from the solvent, respectively. All the results were expressed as the average value of at least four independent measurements. Through analysis of the resulting force vs depth curves, the advancing and receding contact angles as well as the dynamic contact angle hysteresis were obtained. The static contact angles of *n*-alcohols and *n*-alkanes on the surfaces were measured using a KSV Instruments LCD CAM 200 optical contact angle meter at room temperature (23 °C) to calculate the critical surface tensions of the PFPE surfaces from the Zisman method. In the Owens−Wendt−Kaelble (OWK) method, water and *n*-hexadecane were used as polar and nonpolar probe liquids, respectively.

Preparation of Samples for Algal Assays. Free-standing samples with a thickness of $\sim$1 mm were achieved by casting the PFPE macromonomers containing 0.2 wt % of HCPK over a silicon wafer followed by UV irradiation under nitrogen purge for 10 min. To remove any unpolymerized monomers, which if present may have been toxic to the organism used in the bioassays, the samples were continuously extracted by utilizing supercritical CO_2 under 5000 psi and 50 °C for 4 h. After extracting, the free-standing films were secured in racks which were placed in a 30 L tank of deionized water that was recirculated through a carbon filter. After 9 weeks of leaching, the samples were transferred to artificial seawater for 2 h prior to the start of the bioassay. A PDMS elastomer, Silastic-T2 (Dow Corning), cast on glass microscope slides was included as a standard in the assays.[2]

Settlement of Zoospores and Adhesion Strength of Sporelings of *Ulva*. *Ulva* is the most common macroalga (seaweed) that fouls man-made structures including ships. Dispersal of the algae is achieved mainly through the production of zoospores, 5−7 μm in length, which swim in the water column until they find a suitable substrate for settlement. Settlement involves the transition from a swimming spore to an attached, nonmotile spore, which adheres to the substrate through the release of a glycoprotein adhesive.[26] Settled spores rapidly germinate into sporelings (young plants), generally adhere weakly to PDMS-based fouling-release coatings. The spore settlement assay provides information about the antifouling potential of a surface while the sporeling adhesion strength assay indicates the fouling-release potential of a surface.

Zoospores were released from fertile plants of *Ulva linza* and prepared for assays as described previously.[27] In brief, 10 mL of a zoospore suspension (1.0×10^6 spores/mL) was pipetted into individual compartments of polystyrene Quadriperm culture dishes (Greiner), each containing a test surface. The dishes were incubated in darkness at $\sim$20 °C. After 1 h, the slides were gently washed in seawater to remove zoospores that were still swimming and had not settled (attached). After fixation in glutaraldehyde, the density of the zoospores attached to the surface was counted on each of three replicate samples using an image analysis system attached to a fluorescence microscope.[28] Spores were visualized by autofluorescence of chlorophyll. Counts were made for 30 fields of view (each 0.17 mm^2) on each of three replicate samples.

Sporelings were grown on an additional six replicates of each test surface. The procedure followed that described above, but after washing away spores that had not settled, the attached spores were cultured in an enriched seawater medium in Quadriperm dishes as described.[29] The medium was refreshed every 2 days, and the sporelings were cultured for 7 days. Sporeling

biomass was determined in situ by measuring the fluorescence of the chlorophyll, as relative fluorescence units (RFU), contained within the sporelings using a Tecan fluorescent plate reader. The RFU value for each slide was the mean of 70 point fluorescence readings.[29] The strength of the attachment of the sporelings was quantified after exposure to an impact pressure of 32 kPa produced by a calibrated water jet. Percentage removal of biomass was calculated from the before exposure and after exposure RFU readings. One-way analysis of variance and Tukey tests were used to identify significant differences in biomass removal from the surfaces.

Results and Discussion

It is attractive to study the structure/property relationship of fluorinated polymers to create the next generation of environmentally friendly antifouling/fouling-release coatings in a variety of applications ranging from ship hull coatings to long in-dwelling medical devices. To determine the effect of the chemical structure on the fouling-release performance, telechelic PFPE diols were modified with polymerizable methacrylate and styrene end groups via a reaction between the hydroxyl end groups and isocyanatoethyl methacrylate to form urethane linkages or benzyl chloride to form ether linkages, respectively (Scheme 1). To study the effect of cross-link density on the surface and bulk properties of the elastomers, PFPE diols with longer chain were formed via a chain extension reaction of the 4 kg/mol PFPE diol with isophorone diisocyanate (IPDI) in a proper stoichiometry. The resulting chain extended PFPE diols were then further modified with methacrylate end groups to form photochemically curable macromonomers. As seen in Scheme 1, the 2×4 and 3×4 kg/mol PFPE-DMA macromonomers were obtained by initially setting the molar ratio of PFPE diol to IPDI to 2:1 and 3:2, respectively. The effect of the functional end group structure was studied by forming the 4 kg/mol distyrenyl-modified PFPE macromonomer (4 kg/mol sPFPE). To further explore the effect of styrene on properties of the materials, a fluorinated styrenesulfonic ester (SS) was mixed with the sPFPE precursor to form a homogeneous sPFPE-SS solution under heating up to 45 °C. All of the obtained PFPE macromonomers could be photochemically cured to form elastomeric films under UV irradiation in one step.

It is well-known that PFPE exhibit exceptionally high chemical and thermal stabilities imparted by the strong C−F and C−C bonds and shielding of the polymer backbone by the sheath of nonbonding electrons from the fluorine atoms.[30] The thermal stability of all of the fully cured PFPE films was investigated by TGA with a heating rate of 10 °C/min under a nitrogen atmosphere. As shown in Figure 1, all of the samples maintained consistent weights up to 250 °C. The 4 kg/mol PFPE-based elastomeric materials (4 kg/mol PFPE-DMA, 4 kg/mol sPFPE, and 10% sPFPE-SS) were observed to have higher decomposition temperatures (defined as the 5% weight loss) than the 1 kg/mol PFPE-DMA and the chain extended PFPE-DMAs. For example, a decomposition temperature of 333 °C for the 4 kg/mol PFPE-DMA and 350 °C for the 4 kg/mol sPFPE-SS sample were recorded while the 1 kg/mol PFPE-DMA has a decomposition temperature of only 274 °C. For the chain-extended PFPE-DMA samples, the decomposition temperature was observed to decrease, from 333 °C for the non-chain-extended 4 kg/mol PFPE-DMA, to 306 °C for the 2×4 kg/mol PFPE-DMA chain-extended sample, to 283 °C for the 3×4 kg/mol PFPE-DMA sample. This loss in thermal stability is likely due to the breaking of the urethane linkage between the 4 kg/mol PFPE segments.

The DSC curves of the fully cured PFPE samples are plotted in Figure 2. In general, two glass transition temperatures (T_g's) were found. A similar observation was previously reported by Malucelli et al. for a related system.[31] The first glass transition (T_{g1}) at ~0 °C is believed to be related to the hydrocarbon domains of

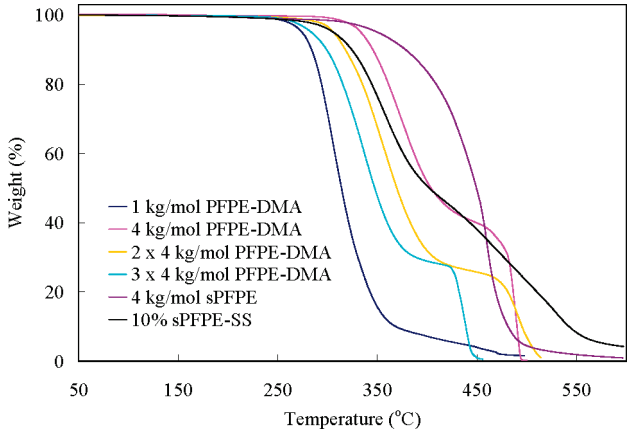

Figure 1. TGA curves of fully cured PFPE films.

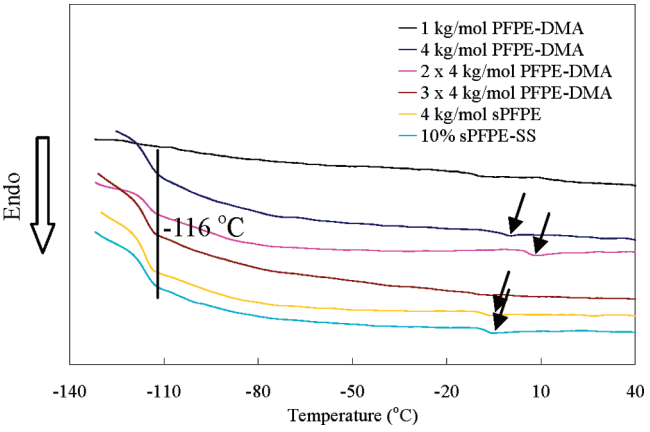

Figure 2. DSC spectra of fully cured PFPE films.

the PFPE networks, and the second glass transition (T_{g2}) at ~−116 °C corresponds to the fluorocarbon moieties. Without the urethane linkage groups in the polymer matrix, the T_{g1} of the cured 4 kg/mol sPFPE sample is slightly lower than that of the PFPE-DMA samples presumably due to a decreased physical cross-linking formed by hydrogen bonds. Compared to that of the 4 kg/mol sPFPE sample, a low content (10%) of fluorinated styrenesulfonic ester monomer in the sPFPE-SS copolymer sample shows no significant impact on the T_g as shown in Figure 2. The detailed T_g information on the studied PFPE samples has been summarized in Table 1.

Because of the high cross-link density, it is difficult to obtain the T_g information for the cured 1 kg/mol PFPE-DMA sample by using DSC. However, detailed information can be collected by using the more sensitive DMTA method as shown in Figure 3. Two T_g's were clearly observed for the 1 kg/mol PFPE-DMA sample. A pronounced T_{g1}, at 54.5 °C, was assigned to the methacrylate cross-linking end groups of the PFPE domains, and a secondary relaxation (T_{g2}) at −80.4 °C was assigned to the PFPE domains of the main chains located away from the cross-links. It is surprising to find that the DMTA trace of the higher molecular weight 4 kg/mol PFPE-DMA sample is very different from that of the 1 kg/mol PFPE-DMA sample. The T_{g1} for the cross-linked methacrylate end groups of the 4 kg/mol PFPE-DMA elastomer was shifted down by almost 25 °C compared to the 1 kg/mol PFPE-DMA samples: from 54.5 to 30 °C. Additionally, the predominant peak for T_{g2} at −130.1 °C, assigned to the PFPE segments between the cross-linked methacrylate end groups, is almost 50 °C lower than that of the 1 kg/mol PFPE-DMA elastomer. Interestingly, the activity for the hydrocarbon domains

Table 1. Summary of Thermal Analysis and Young's Modulus

		DSC (°C)		DMTA (°C)		
	decomposition temp (°C)	T_{g2}	T_{g1}	T_{g2}	T_{g1}	modulus (MPa)
1 kg/mol PFPE-DMA	274	n/a	n/a	−80.4	54.5	89.9 ± 10.0
4 kg/mol PFPE-DMA	333	−115.3	0	−130.2	30.0	7.0 ± 0.3
2 × 4 kg/mol PFPE-DMA	306	−116.0	6.6	−131.8	−17.8	3.6 ± 0.2
3 × 4 kg/mol PFPE-DMA	283	−116.3	n/a	−131.5	−35.8	1.5 ± 0.1
4 kg/mol sPFPE	350	−116.7	−7.6	−132.0	n/a	2.2 ± 0.1
10% sPFPE-SS	306	−116.5	−6.8	−131.5	n/a	2.6 ± 0.1

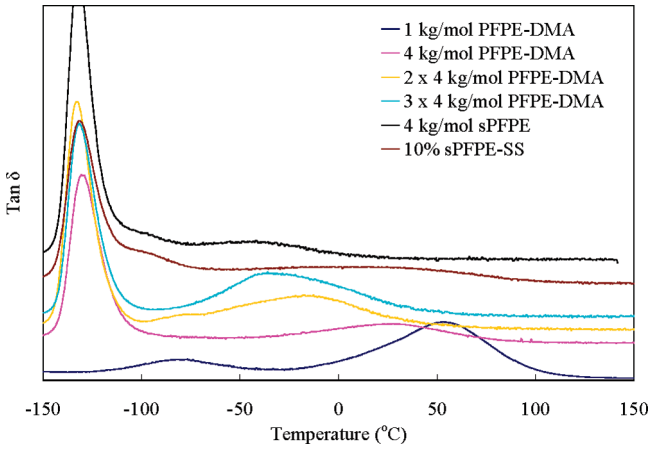

Figure 3. DMTA spectra of fully cured PFPE films.

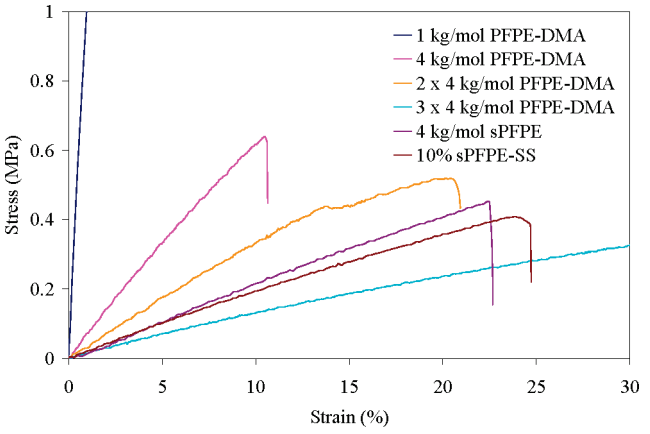

Figure 4. Stress−strains curves of cross-linked PFPE networks by Instron.

is much weaker compared with the PFPE moieties due to the decreased concentration of the methacrylate end groups. For the chain-extended PFPE-DMA samples, the predominant T_{g2} peak for the PFPE segments remained unchanged at ∼−131 °C while the T_{g1} for the hydrocarbon domains gradually shifted to −35.8 °C as the molecular weight was increased. This indicates that the short urethane ether methacrylate segments possess a relatively higher mobility in the less cross-linked PFPE matrix. Similarly, a single T_g at −132 °C was clearly observed as the relaxation of the PFPE moieties for the 4 kg/mol sPFPE-based samples. Instead of a peak corresponding to the hydrocarbon domains in the higher temperature region, a broad signal for the 4 kg/mol sPFPE and 10% sPFPE-SS samples was observed, making it difficult to define the peak maxima.

It is often desirable to tune the modulus to fit the materials to various applications. In this study, control over the modulus of the cured PFPE materials was induced by varying molecular weights and functional end groups, which both are thought to change the cross-link density of PFPE matrix. The higher molecular weight PFPE macromonomers will result in cross-linked networks with lower cross-link densities upon UV curing. Additionally, strong hydrogen-bond associations between the urethane linkage groups of the individual PFPE chain were thought to increase the intermolecular interactions and further enhance the mechanical strength of the cross-linked networks.[32] The modulus was determined by the slope of the initial linear region of the stress−strain curve (∼2% elongation). As shown in Figure 4, the modulus for the 1 kg/mol PFPE-DMA sample is 90 MPa. As the molecular weight of the PFPE-DMA was increased, the modulus was gradually decreased due to the decreased chemical and physical cross-link density. Specifically, for the highest molecular weight sample, 3 × 4 kg/mol PFPE-DMA, the modulus was only 1.5 MPa. The modulus of this system is tunable between 1.5 and 90 MPa through the curing of blends with the different macromonomers at variable composition ratios. For example, the cured 50:50 by weight blend of the 1 and 4 kg/mol PFPE-DMAs had a modulus of 34 MPa. It is interesting that the modulus of this system can be varied while the thermal, optical, and surface properties remain similar because all of the components of the blends have similar chemical structures. Without the urethane linkage groups in the cured PFPE matrix to form strong hydrogen bonds, the modulus of the 4 kg/mol sPFPE sample is much lower compared to that of the 4 kg/mol PFPE-DMA sample. By incorporating 10 wt % of the rigid styrenesulfonic ester monomer (SS) into the 4 kg/mol sPFPE matrix, the modulus of the resulting copolymer network was slightly increased from 2.2 to 2.6 MPa; however, it is still much lower than the 4 kg/mol PFPE-DMA sample.

The performance of coating materials is often dictated by surface and interfacial properties such as wettability and adhesion. The contact angle and the surface tension are determined by the competition of these two factors.[33] In this study, the advancing and receding contact angles at the air interfaces of the samples were measured by the Wilhelmy plate method.[25] The dynamic contact angle hysteresis curves for all of the PFPE-DMAs were recorded by a tensiometer, as seen in Figure 5 with the contact angle as a function of immersion depth. The results indicate that all of the PFPE surfaces are highly hydrophobic with a water advancing contact angle greater than 110° and a receding contact angle from 76° to 39°. This large difference in the advancing and receding contact angles subsequently led to a large contact angle hysteresis. The dynamic contact angle values are summarized in Table 2. For the series of PFPE-DMA samples, as the molecular weight increased, i.e., the cross-link density decreased, the advancing contact angles slightly increased, from 117° for the 1 kg/mol PFPE-DMA sample to 126° for the 3 × 4 kg/mol PFPE-DMA sample. Simultaneously, the receding contact angles dramatically decreased from 76° to 39°. As a result, it caused a large disparity on the contact angle hysteresis. Particularly, the contact angle hysteresis is only 39° for the 1 kg/mol PFPE-DMA surface while it increased to 56° for the 4 kg/mol PFPE-DMA sample which possesses a decreased cross-link density. The contact angle hysteresis increased to 74° for the 2 × 4 kg/mol PFPE-DMA sample with an even lower cross-link density and

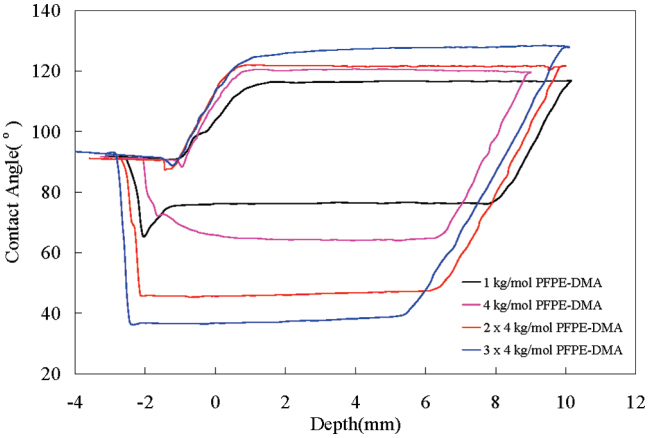

Figure 5. Dynamic contact angle hysteresis of the PFPE-DMAs given by dynamic surface tensiometry (DST).

Table 2. Dynamic Contact Angle and Contact Angle Hysteresis

	dynamic contact angle (deg)		
	advancing	receding	hysteresis
1 kg/mol PFPE-DMA	117.4 ± 0.8	76.0 ± 1.0	38.9
4 kg/mol PFPE-DMA	120.4 ± 0.5	64.6 ± 1.1	55.8
2 × 4 kg/mol PFPE-DMA	121.6 ± 0.5	47.5 ± 4.4	74.1
3 × 4 kg/mol PFPE-DMA	126.6 ± 1.5	38.6 ± 2.9	80.6
4 kg/mol sPFPE	113.7 ± 1.9	73.8 ± 1.6	39.9
10% sPFPE-SS	116.7 ± 0.8	76.0 ± 1.8	40.7

further increased to 81° for the 3 × 4 kg/mol PFPE-DMA sample. According to the literature, the main factors contributing to contact angle hysteresis can be the surface roughness, swelling of the studied surface, and surface reorganization.[34] It is known that PFPE is very chemically stable with a negligible water uptake of less than 1% after 2 weeks soaking in water.[35] Our previous studies also indicated that all of the PFPE surfaces cured in this manner were ultraflat with a surface roughness less than 1 nm.[36] The most plausible contribution to the hysteresis in this system is therefore from the surface group reorganization.

The dynamic contact angle hysteresis can be explained through a series of reversible, short-range interactions of the polar segments in the polymer backbone with water on the surface. The high advancing contact angles are observed as water comes in contact with the fluorocarbon dominant polymer/air interface. Once the surface is wetted, the polymer will reorganize the interface by rotating or relaxing the polar hydrophilic functionalities such as the urethane segments in the end groups of the PFPE chains to interact with water, which can be accomplished by both forming hydrogen bonds and enhancing the dispersion interaction with water. Additionally, the hydrogen atoms of the $-CF_2CH_2O-$ units adjacent to the PFPE segments are acidic, which allows for them to participate in similar polar interactions. Thus, the interaction of these functionalities with water would be favored, allowing the water molecules to penetrate and further facilitating the migration of the polar groups toward the interface. A low receding contact angle is an indication of significant surface reorganization, which results in high contact angle hysteresis.[18] Compared with the chain-extended PFPE-DMA samples, the lower molecular weight 1 kg/mol PFPE-DMA sample has a relatively higher cross-link density. In this case, the polymer chains were highly constrained, thus making the chain rotation or reorganization on the surface of any polar moieties such as the oxygen and the urethane groups very difficult. The mobility of the polymerized polar urethane ether methacrylate end groups of the PFPE samples was indicated by the corresponding glass transition temperature (T_{g1}). As seen in

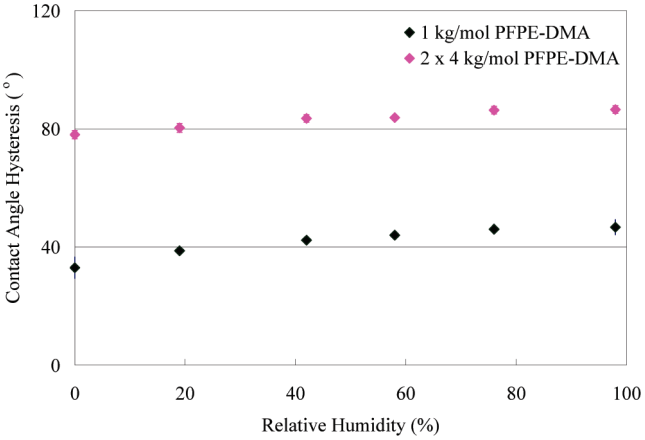

Figure 6. Contact angle hysteresis observations of PFPE films cured under variable humidity environments.

Table 1, the 1 kg/mol PFPE-DMA sample possesses a higher T_{g1} (54.5 °C) compared to all of the other PFPE-DMA samples. It suggests the polymerized polar end groups are constrained and possess a low mobility, making it difficult for the segments to initiate the short-range relaxation and rotation needed to reorganize the surface. As a result, the material has a smaller contact angle hysteresis.

Besides the cross-link density, the impact of the relative humidity during curing on the contact angle hysteresis was also investigated. Previous studies have shown the adsorption of water on the PFPE surface improves the mobility of the PFPE molecules,[37] but it not clear whether the relative humidity during the curing step has an effect on the enrichment of polar groups to the PFPE/air interface, resulting in a large contact angle hysteresis. To this end, a humid environment inside the UV chamber was induced by passing a nitrogen purge stream through a bubbler containing LiCl solution at desired concentrations.[24] The dynamic contact angle hysteresis was compared on the fully cured systems of the 1 kg/mol PFPE-DMA and the 2 × 4 kg/mol PFPE-DMA films.

As shown in Figure 6, the data were plotted as the relationship of the contact angle hysteresis with the relative humidity. The hysteresis was seen to increase as the relative humidity was increased. This result supports the hypothesis that as the humidity in the chamber is increased, more polar groups migrate to the PFPE surface and are locked into place during UV curing. This process would facilitate the penetration of water into the PFPE surface, resulting in a further increase in the contact angle hysteresis. Specifically, in this study the hysteresis was increased from 33° to 46° for the 1 kg/mol PFPE-DMA sample and from 78° to 86° for the 2 × 4 kg/mol PFPE-DMA sample. A large disparity in hysteresis as a function of humidity has not been observed on these photochemically cured PFPE surfaces, compared with those previously reported for thermally cured PFPE terpolymer surfaces, which consisted of more polar acrylate and epoxide moieties containing monomers. An increase of up to 40° in the hysteresis was observed by varying the relative humidity from 0% to ~100%.[18] The increase observed here for both PFPE-DMAs is ~10°. This smaller change in hysteresis is thought to be a result of the limited number of polar groups present in these perfluorinated polymers and the high cross-link density, which effectively constrains the chain rotation and reorganization by immobilizing the chains during the curing step.

The critical surface tensions of the studied PFPE surfaces were quantified by the Zisman method by measuring static contact angles of a series of *n*-alcohols on the fully cured PFPE elastomer surfaces.[38,39] On the basis of the linear relationship between cos θ (θ, the static contact angle) and the corresponding surface tension

Table 3. Summary of Surface Tensions

	critical surface tension[a] (mN/m)		surface tension[b] (mN/m)		
	alcohols	alkanes	γ_S^d	γ_S^p	γ_S
1 kg/mol PFPE-DMA	14.5 ± 1.6	12.5 ± 0.4	13.6	2.7	16.3
4 kg/mol PFPE-DMA	8.6 ± 1.5	11.4 ± 0.2	11.5	2.4	13.9
2 × 4 kg/mol PFPE-DMA	15.4 ± 0.7	13.6 ± 0.7	11.8	1.6	13.4
3 × 4 kg/mol PFPE-DMA	16.1 ± 0.5	13.6 ± 0.5	12.7	0.7	13.4
4 kg/mol sPFPE	15.9 ± 0.6	14.8 ± 0.9	13.0	1.3	14.3
10% sPFPE-SS	14.4 ± 0.9	13.5 ± 0.6	12.4	1.4	13.8

[a] Calculated with the Zisman plot method. [b] Calculated with the Owens−Wendt−Kaelble method: γ_S^d = dispersion component, γ_S^p = polar component, γ_S = overall surface tension.

of the probe solvent, the critical surface tension was calculated for each PFPE surface by extrapolation of the linear plot to the point of cos θ = 1, which ranges from 8.6 to 16 mN/m as shown in Table 3. The results are in agreement with previously reported PFPE−urethane cross-linked networks (13−16 mN/m);[40] however, as dynamic surfaces, it is difficult to obtain accurate critical surface tension values for the PFPE materials because the surfaces easily undergo environment-dependent surface reorganization.[41] As a result of the surface reorganization, the surface hydrophilicity and hence the critical surface tension may change when probe liquids of variable polarity are used. To study the effect of the polarity of the probe solvent on the critical surface tension, the critical surface tension was recalculated based on Zisman plot method using less polar *n*-alkanes as probe liquids. The surface tension values are summarized in Table 3 and compared to those values obtained from the polar *n*-alcohols. Generally, the critical surface tensions show a similar trend on these surfaces when two different sets of probe liquids are used. However, the critical surface tension obtained from the hydrophobic alkane probe liquids is lower than that obtained from the more polar alcohol probe liquids on the same surface, except for the 4 kg/mol PFPE-DMA sample. This is likely attributed to the fact that the polar alcohols are more effective at driving the PFPE surface reorganization by forming hydrogen bonds and dipolar interactions with the polar segments such as the oxygen and urethane groups at the uppermost PFPE surface.

To distinguish the contribution of the different interaction components to the surface tension such as the van der Waals dispersive forces, dipole interactions, hydrogen bonds, etc., Owens, Wendt, and Kaelble (OWK) defined the solid surface tension (γ_S) as the sum of the dispersion component (γ_S^d) and the polar component (γ_S^p)and combined it with the Young's equation to yield[42,43]

$$\gamma_L = 2\frac{(\gamma_S^d\gamma_L^d)^{1/2} + (\gamma_S^p\gamma_L^p)^{1/2}}{1+\cos\theta} \quad (1)$$

where θ is the static contact angle, γ_L is the surface tension of a probe liquid, and γ_L^d and γ_L^p are the dispersive component and the polar component of the liquid surface tension, respectively. By measuring the contact angles of two different probe liquids (one polar and one nonpolar) on each surface, the overall solid surface tension can be calculated based on the equation. In this study, water and *n*-hexadecane were used as the polar and nonpolar probe liquids, which are γ_L^d = 27.6 mN/m, γ_L^p = 0 mN/m for *n*-hexadecane and γ_L^d = 21.8 mN/m, γ_L^p = 51.0 mN/m for water, respectively. The surface tensions calculated from the OWK method are listed in Table 3. The overall surface tensions are seen to be 13−14 mN/m for all tested PFPE surfaces, except that the 1 kg/mol PFPE-DMA has a relatively higher surface tension of 16.3 mN/m. These results are in reasonable agreement with those given by the Zisman method. As expected, the dispersive component (11.5−13.6 mN/m) is the main contributor to the surface tension while the polar surface tension component was only 5−17% of the total surface tension. Particularly for the 1 and 4 kg/mol PFPE-DMA samples, the polar component contributes in a relatively high percentage of 17% to the total surface tension. It is interesting to observe that for the PFPE-DMA series of samples the percent contribution of the polar component to the surface tension decreased as the molecular weight of the PFPE-DMA precursors increased. This is understandable since the lower molecular weight 1 and 4 kg/mol PFPE-DMA samples contain more polar urethane ether methacrylate end groups in the cross-linked PFPE surfaces. The surface tensions calculated from the OWK method are correlated to the observation from the advancing contact angle measurements. A lower advancing contact angle was expected on the 1 kg/mol PFPE-DMA surface because the surface possesses a relatively larger contribution from the polar component.

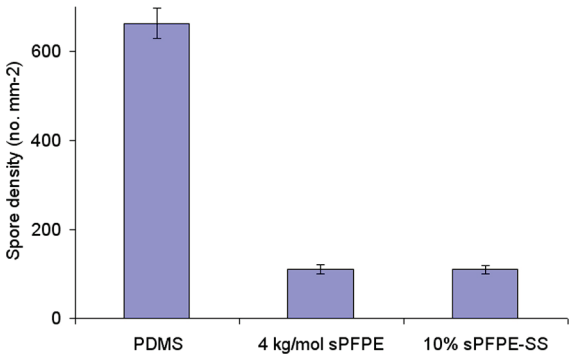

Figure 7. Density of attached spores of *Ulva* on PDMS (Silastic T2) and PFPE elastomers after a 1 h settlement period. Each bar is the mean of 90 counts, 30 on each of 3 replicate slides. Error bars show 95% confidence limits.

Biofouling Tests. *Settlement of Zoospores and Adhesion Strength of Sporelings of Ulva*. Monolithic samples of the 4 kg/mol PFPE-DMA, 4 kg/mol sPFPE, and 10% sPFPE-SS were tested for *Ulva* spore settlement and sporeling removal. Previously conducted preliminary tests showed that only the 4 kg/mol sPFPE and 10% sPFPE-SS increased performance compared to PDMS standards.[44] This is most likely because the 4 kg/mol PFPE-DMA elastomer has a relatively high modulus and a large contact angle hysteresis even though the material possesses a similar surface tension to the 4 kg/mol sPFPE and 10% sPFPE-SS samples based on the OWK method. Previous studies with PDMS showed that the removal of sporelings of *Ulva* was increased from coatings as the elastic modulus decreased. Furthermore, biomass removal was higher for coatings with an elastic modulus of 2.7 MPa compared to 9.4 MPa.[45]

Spore settlement densities were substantially lower on the 4 kg/mol sPFPE and 10% SS-sPFPE monoliths than on the PDMS standards (Figure 7), but there was no significant difference between the 4 kg/mol sPFPE and the 10% sPFPE-SS

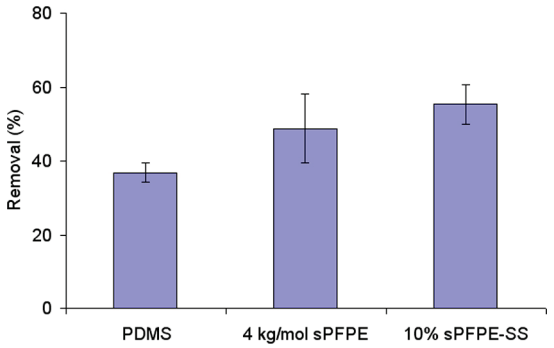

Figure 8. Percentage removal of sporeling biomass from PDMS (Silastic T2) and PFPE elastomers following exposure to an impact pressure of 32 kPa produced by a water jet. Each bar is the mean percentage removal from six replicate slides. Error bars show the standard error of the mean derived from arcsine transformed data.

surfaces. Microscopic observations indicated that the attached spores were normal and healthy on both PFPE samples. Previous studies have indicated that higher numbers of spores settle on hydrophobic compared to hydrophilic surfaces,[46−48] so the present results that show a low settlement density on the hydrophobic PFPE surfaces is not typical, but nevertheless a highly desirable characteristic for a potential antifouling coating.

The spores were cultured on the test surfaces for 7 days, during which time they germinated and grew into sporelings. Although biomass production was lower on the 4 kg/mol sPFPE and 10% sPFPE-SS surfaces than on the PDMS standard reflecting the lower spore settlement density, all of the surfaces were covered by a green lawn of sporelings after 7 days. The strength of attachment of the sporelings was similar on both of the PFPE monoliths and on the PDMS standards (Figure 8). One-way analysis of variance showed that there was no significant difference in removal from the three surfaces (F 2, 15 = 2.67 $P > 0.05$). Commercial fouling-release coatings based on PDMS show weak attachment strength for a wide range of fouling organisms.[49,50] The fouling-release characteristics of these materials are attributed to their smooth surfaces, low modulus, hydrophobicity, and properties of surface reconstruction which are all qualities shared with the PFPE elastomers.

Conclusion

A series of novel perfluoropolyethers have been synthesized via a solventless process using liquid precursors that are capable of being photochemically cross-linked into elastomeric networks. The structure/property relationships were systematically investigated as a function of end groups, molecular weight, and content of a comonomer. Generally two glass transitions were observed for these PFPE-based materials with the first transition assigned to the hydrocarbon domains and the second transition at lower temperature assigned to the fluorinated domains. Through a SAXS study, the domain spacing was estimated to be 3.3 nm for the 1 kg/mol PFPE-DMA sample and ∼5.2 nm for the 4 kg/mol PFPE-base samples (see Supporting Information). It was demonstrated that the moduli of the fully cured PFPE samples can be tuned by using precursors with various chain lengths to vary the cross-link density. The contact angle hysteresis and the critical surface tension of these films have been studied. Both the cross-link density and the curing environment humidity show effect on the chain reorganization and the contact angle hysteresis. A lower cross-link density or more humid cure environment is likely to drive more polar groups toward the surface and facilitate chain reorganization that results in a larger contact angle hysteresis. The PFPE materials with low surface tension, Young's modulus, and contact angle hysteresis show decreased zoospore settlement and comparable sporeling removal performance to PDMS elastomer standard material. The ease of fabrication, the ability to tune the properties, and the promising fouling-release performance coupled with potentially greater service lifetime could provide opportunities for these PFPE elastomers to be utilized as fouling-release coatings in marine environments.

Acknowledgment. This research is supported by the Office of Naval Research under Awards #N00014-02-1-0185 (J.M.D.) and #N00014-05-1-0134 (J.A.C. and M.E.C.) as well as the NSF-STC Center for Environmentally Responsible Solvents and Processes (CHE-9876674) for shared facilities. Parts of this work were carried out in the University of Minnesota I.T. Characterization Facility, which receives partial support from NSF through the NNIN program.

Supporting Information Available: SAXS results. This material is available free of charge via the Internet at http://pubs.acs.org.

References and Notes

(1) IMO, International Convention on the Control of Harmful Antifouling Systems on Ships AFS/CONF/26; **2001**, p 18.
(2) Schumacher, J. F.; Carman, M. L.; Callow, M. E.; Finlay, J. A.; Brennan, A. B. *Biofouling* **2007**, *23*, 55–62.
(3) Stein, J.; Truby, K.; Darkangelo-Wood, C.; Stein, J.; Gardner, M.; Swain, G.; Kavanagh, C.; Kovach, B.; Schultz, M.; Wiebe, D.; Holm, E.; Montemarano, J.; Wendt, D.; Smith, C.; Meyer, A. *Biofouling* **2003**, *19* (Supplement), 71−82.
(4) Majumdar, P.; Lee, E.; Patel, N.; Ward, K.; Stafslien, S. J.; Daniels, J.; Boudjouk, P.; Callow, M. E.; Callow, J. A.; Thompson, S. E. *Biofouling* **2008**, *24*, 185–200.
(5) Beigbeder, A.; Degee, P.; Conlan, S. L.; Mutton, R. J.; Clare, A. S.; Pettitt, M. E.; Callow, M. E.; Callow, J. A.; Dubois, P. *Biofouling* **2008**, *24*, 291–302.
(6) Stein, J.; Truby, K.; Darkangelo-Wood, C.; Takemori, M.; Vallance, M.; Swain, G.; Kavanagh, C.; Kovach, B.; Schultz, M.; Wiebe, D.; Holm, E.; Montemarano, J.; Wendt, D.; Smith, C.; Meyer, A. *Biofouling* **2003**, *19*, 87–94.
(7) Baier, R. E.; Loeb, G. I.; Wallace, G. A. *Fed. Proc.* **1971**, *30*, 1523–1528.
(8) Brady, R. F.; Singer, I. L. *Biofouling* **2000**, *15*, 73–81.
(9) Kim, J.; Chisholm, B. J.; Bahr, J. *Biofouling* **2007**, *23*, 113–120.
(10) Kim, E.; Xia, Y.; Zhao, X.-M.; Whitesides, G. M. *Adv. Mater.* **1997**, *9*, 651–654.
(11) Schultz, P. M. *Biofouling* **2007**, *23*, 331–341.
(12) Kobayashi, H.; Owen, M. J. *Trends Polym. Sci.* (*Cambridge, U. K.*) **1995**, *3*, 330–335.
(13) Gudipati, C. S.; Finlay, J. A.; Callow, J. A.; Callow, M. E.; Wooley, K. L. *Langmuir* **2005**, *21*, 3044–3053.
(14) Hexemer, A.; Sivaniah, E.; Kramer, E. J.; Xiang, M.; Li, X.; Fisher, D. A.; Ober, C. K. *J. Polym. Sci., Part B* **2004**, *42*, 411–420.
(15) Krishnan, S.; Ayothi, R.; Hexemer, A.; Finlay, J. A.; Sohn, K. E.; Perry, R.; Ober, C. K.; Kramer, E. J.; Callow, M. E.; Callow, J. A.; Fischer, D. A. *Langmuir* **2006**, *22*, 5075–5086.
(16) Thanawala, S. K.; Chaudhury, M. K. *Langmuir* **2000**, *16*, 1256–1260.
(17) Marabotti, I.; Morelli, A.; Orsini, L. M.; Martinelli, E.; Galli, G.; Chiellini, E.; Lien, E. M.; Pettitt, M. E.; Callow, J. A.; Conlan, S. L.; Mutton, R. J.; Clare, A. S.; Kocijan, A.; Donik, C.; Jenko, M. *Biofouling* **2009**, *25*, 481–493.
(18) Yarbrough, C.; Rolland, J. P.; DeSimone, J. M.; Callow, M. E.; Finlay, J. A.; Callow, J. A. *Macromolecules* **2006**, *39*, 2521–2528.
(19) Fouassier, J. P.; Rabek, J. F. *Radiation Curing in Polymer Science and Technology*; Elsevier: London, 1993; Vols. I−IV.
(20) Roffey, C. G. *Photopolymerization of Surface Coatings*; Wiley: New York, 1982.
(21) Rolland, J. P.; VanDam, R. M.; Schorzman, D. A.; Quake, S. R.; DeSimone, J. M. *J. Am. Chem. Soc.* **2004**, *126*, 2322–2323.
(22) Rolland, J. P. Functional Perfluoropolyethers for Novel Applications. Doctorate Dissertation, University of North Carolina at Chapel Hill, **2004**; p 160.

(23) Zhou, Z.; Dominey, R. N.; Rolland, J. P.; Maynor, B. W.; Pandya, A. A.; DeSimone, J. M. *J. Am. Chem. Soc.* **2006**, *128*, 12963–12972.
(24) Robinson, R. A. *Trans. Faraday Soc.* **1945**, *41*, 756–758.
(25) Adamson, A. M.; Gast, A. P. In *Physical Chemistry of Surface*, 6th ed.; John Wiley and Sons: New York, 1993; Vol. *49*, pp 1−73.
(26) Callow, J. A.; Callow, M. E. The Ulva Spore Adhesive System. In *Biological Adhesives*; Smith, A. M., Callow, J. A., Eds.; Springer-Verlag: Berlin, Heidleberg, 2006; pp 63−78.
(27) Callow, M. E.; Callow, J. A.; Pickett-Heaps, J. D.; Wetherbee, R. *J. Phycol.* **1997**, *33*, 938–947.
(28) Callow, M. E.; Jennings, A. R.; Brennan, A. B.; Seegert, C. E.; Gibson, A.; Wilson, L.; Feinberg, A.; Baney, R.; Callow, J. A. *Biofouling* **2002**, *18*, 237–245.
(29) Finlay, J. A.; Fletcher, B. R.; Callow, M. E.; Callow, J. A. *Biofouling* **2008**, *24*, 219–225.
(30) Scheirs, J. *Modern Fluoropolymers*; John Wiley & Sons, Ltd.: New York, 1997.
(31) Priola, A. B., R.; Malucelli, G.; Pollicino, A.; Tonelli, C.; Simeone, G. *Macromol. Chem. Phys.* **1997**, *198*, 1893–1907.
(32) Yilgor, E.; Yilgor, I. *Polymer* **2001**, *42*, 7953–7959.
(33) Kinlock, A. K. *Adhesion and Adhesive, Surface and Technology*; Chapman and Hall: New York, 1987; Chapter 2.
(34) Erbil, H. Y.; McHale, G.; Rowan, S. M.; Newton, M. I. *Langmuir* **1999**, *15*, 7378–7385.
(35) Hu, Z.; Chen, L.; Betts, D. E.; Pandya, A.; Hillmyer, M. A.; DeSimone, J. M. *J. Am. Chem. Soc.* **2008**, *130*, 14244–14252.
(36) Maynor, B. W.; LaRue, I.; Hu, Z.; Rolland, J. P.; Pandya, A.; Fu, Q.; Liu, J.; Spontak, R. J.; Sheiko, S. S.; Samulski, R. J.; Samulski, E. T.; DeSimone, J. M. *Small* **2007**, *3*, 845–849.
(37) O'Connor, T. M.; Back, Y. R.; Jhon, M. S.; Min, B. G.; Yoon, D. Y.; Karis, T. E. *J. Appl. Phys.* **1996**, *79*, 5788–5790.
(38) Fox, H. W.; Zisman, W. A. *J. Colloid Sci.* **1950**, *5*, 514–531.
(39) Lama, C. N. C.; Wua, R.; Lia, D.; Haira, M. L.; Neumann, A. W. *Adv. Colloid Interface Sci.* **2002**, *96*, 169–191.
(40) Turri, S.; Radice, S.; Canteri, R.; Speranza, G.; Anderle, M. *Surf. Interface Anal.* **2000**, *29*, 873–886.
(41) Martinelli, E.; Menghetti, S.; Galli, G.; Glisenti, A.; Krishnan, S.; Paik, M. Y.; Ober, C. K.; Smilgies, D.-M.; Fischer, D. A. *J. Polym. Sci., Part A: Polym. Chem.* **2009**, *47*, 267–284.
(42) Owens, D. K.; Wendt, R. C. *J. Appl. Polym. Sci.* **1969**, *13*, 1741–1747.
(43) Kaelble, D. H. *J. Adhes.* **1970**, *2*, 66–81.
(44) Unpublished results.
(45) Chaudhury, M. K.; Finlay, J. A.; Chung, J. Y.; Callow, M. E.; Callow, J. A. *Biofouling* **2005**, *21*, 41–48.
(46) Callow, M. E.; Callow, J. A.; Ista, L. K.; Coleman, S. E.; Nolasco, A. C.; López, G. P. *Appl. Environ. Microbiol.* **2000**, *66*, 3249–3254.
(47) Schilp, S.; Kueller, A.; Rosenhahn, A.; Grunze, M.; Pettitt, M.; Callow, M. E.; Callow, J. A. *Biointerphases* **2007**, *2*, 143–150.
(48) Finlay, J. A.; Krishnan, S.; Callow, M. E.; Callow, J. A.; Dong, R.; Asgill, N.; Wong, K.; Kramer, E. J.; Ober, C. K. *Langmuir* **2008**, *24*, 503–510.
(49) Swain, G. E. Redefining antifouling coatings. Paint Coatings Europe, July **1999**; pp 18−25.
(50) Kavanagh, C. J.; Schultz, M. P.; Swain, G. W.; Stein, J.; Truby, K.; Darkangelo-Wood, C. *Biofouling* **2001**, *17*, 155–167.